CLINICAL AND VACCINE IMMUNOLOGY, Feb. 2008, p. 235–242 Vol. 15, No. 2
1556-6811/08/$08.00+0 doi:10.1128/CVI.00335-07

Impact of Protein Shedding on Detection of *Mycobacterium avium* subsp. *paratuberculosis* by a Whole-Cell Immunoassay Incorporating Surface-Enhanced Raman Scattering▽

Betsy Jean Yakes,[1]† Robert J. Lipert,[1] John P. Bannantine,[2] and Marc D. Porter[1]*

Departments of Chemistry and Chemical and Biological Engineering, Ames Laboratory-USDOE, and Institute for Combinatorial Discovery, Iowa State University, Ames, Iowa 50011,[1] and USDA/ARS/National Animal Disease Center, Bacterial Diseases of Livestock Research Unit, Ames, Iowa 50010[2]

Received 14 August 2007/Returned for modification 11 October 2007/Accepted 29 November 2007

The etiological agent of Johne's disease is *Mycobacterium avium* subsp. *paratuberculosis*. Controlling the spread of this disease is hindered by the lack of sensitive, selective, and rapid detection methods for *M. avium* subsp. *paratuberculosis*. By using a recently optimized sandwich immunoassay (B. J. Yakes, R. J. Lipert, J. P. Bannantine, and M. D. Porter, Clin. Vaccine Immunol. 15:227–234, 2008), which incorporates a new monoclonal antibody for the selective capture and labeling of *M. avium* subsp. *paratuberculosis* and surface-enhanced Raman scattering for sensitive readout, detection limits of ~630 and ~740 *M. avium* subsp. *paratuberculosis* cells/ml are achieved in phosphate-buffered saline and whole milk samples, respectively, after spiking with heat-treated *M. avium* subsp. *paratuberculosis*. Surprisingly, these detection limits are 3 orders of magnitude lower than expected based on theoretical predictions. Experiments designed to determine the origin of the improvement revealed that the major membrane protein targeted by the monoclonal antibody was present in the sample suspensions as shed protein. This finding indicates that the capture and labeling of shed protein function as a facile amplification strategy for lowering the limit of detection for *M. avium* subsp. *paratuberculosis* that may also be applicable to the design of a wide range of highly sensitive assays for other cells and viruses.

Mycobacterium avium subsp. *paratuberculosis* is responsible for extensive losses in dairy production on a global scale (44). *M. avium* subsp. *paratuberculosis* is also found in other domestic ruminants (e.g., sheep [30, 34] and goats [45, 46]) and wildlife (e.g., deer [21, 31, 32], antelope [6, 17], bison [52], and rabbits [4, 5, 26]). Animals that are afflicted with *M. avium* subsp. *paratuberculosis* progress from silent infection to a subclinical phase with no observable symptoms. Low levels of shedding during this time can nonetheless lead to the transmission of *M. avium* subsp. *paratuberculosis* throughout a herd. Unfortunately, once the physical symptoms associated with the clinical and advanced disease phases (e.g., weight loss and chronic diarrhea) become evident, the disease may already be well established.

As part of a strategy to control the spread of this disease, methods are needed to detect *M. avium* subsp. *paratuberculosis* in its earliest stages of progression. To this end, the detection method must be sensitive, rapid, field deployable, and cost-effective. It must also be selective for *M. avium* subsp. *paratuberculosis* over other bacteria typically found in the types of samples analyzed (e.g., milk and feces). Currently available methods fall short in meeting these combined goals. For example, bacteriologic culturing is lengthy (12 to 16 weeks) (http://johnes.vetmed.wisc.edu), serological tests lack sufficient sensitivity for detection at subclinical levels (8–10, 12, 42, 49), and gamma interferon (24) and nucleic acid probe (11, 18) determinations can be limited by low specificity. PCR-based methods may also suffer from false-negative results in complex matrices like milk (48). In the companion paper (54), a method based on surface-enhanced Raman scattering (SERS) for the detection of sonicated *M. avium* subsp. *paratuberculosis* in less than 24 h was designed and optimized and yielded a limit of detection of ~500 bacilli/ml in a buffer matrix and ~1,000 bacilli/ml in a milk matrix. The work herein examines the extension of this method to the analysis of samples containing whole *M. avium* subsp. *paratuberculosis* cells.

SERS has recently been shown to function as a sensitive detection method in bioanalytical sciences, especially in the area of chip-scale assays (e.g., immunoassays [1, 14, 15, 23, 33, 35, 36, 40, 53, 57] and DNA [7, 19, 22]). The basis of SERS lies in the use of a roughened metal surface to amplify normal Raman scattering, which is an inelastic scattering of light from vibrations in a molecule that undergoes a change in polarizability. The observed enhancement in Raman scattering (up to 10^{14} times) (29) originates from two types of effects: chemical and electromagnetic. The chemical component is based on the formation of a charge transfer state between the metal surface and the adsorbed Raman scattering molecule (50) and is viewed as contributing approximately 2 orders of magnitude to the overall enhancement.

The remainder of the enhancement is derived from electromagnetic effects. When light is incident on a metal surface, conduction electrons in the metal can collectively oscillate. This process, known as surface plasmon resonance, has a wave-

* Corresponding author. Present address: Department of Chemistry, University of Utah, Salt Lake City, UT 84108. Phone: (801) 587-1505. Fax: (801) 585-0575. E-mail: marc.porter@utah.edu.

† Present address: U.S. FDA-CFSAN, 5100 Paint Branch Parkway, College Park, MD 20740.

▽ Published ahead of print on 12 December 2007.

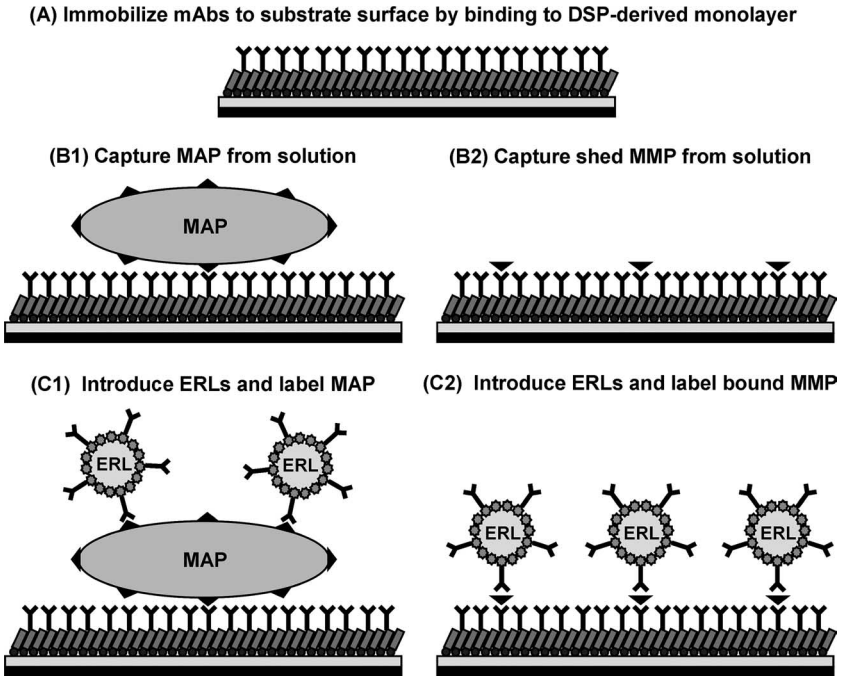

FIG. 1. Schematic of the SERS-based sandwich immunoassay for *M. avium* subsp. *paratuberculosis* (MAP) bacilli and illustration of shed-protein assay format: form capture surface (A), extract antigen from solution (B), and label-bound antigen with a SERS tracer (C).

length dependence that is connected to the nanometric roughness of metallic surfaces and the size and shape of metallic nanoparticles (27). There is also a significant body of theoretical work (20, 28, 29, 41, 56) that has proven invaluable to the fundamental understanding of both enhancement mechanisms.

The method introduced in the companion paper (54) and further developed in this work capitalizes on these theoretical considerations. This approach uses extrinsic Raman labels (ERLs), which feature an adlayer of an intrinsically strong Raman scatterer chemisorbed onto SERS active substrates (i.e., gold nanoparticles) to take advantage of both enhancement effects. When incorporated into a novel SERS-based sandwich immunoassay (Fig. 1), high levels of detection sensitivity can be achieved (e.g., pico- to femtomolar antigen concentrations [23] and single-binding-event [37] detection). In this assay format, a target biolyte (e.g., protein, virus, bacterium, and etc.) is selectively sandwiched between a metal surface and an ERL by a capture antibody and a labeling antibody.

This paper details an evaluation of this assay platform for the detection of whole-cell *M. avium* subsp. *paratuberculosis* bacteria in both buffer and milk matrices. The results showed that the observed detection limit (~700 cells/ml) was 3 orders of magnitude lower than that theoretically predicted ($\sim 8 \times 10^5$ cells/ml). Therefore, experiments that were designed to determine the origin of the improvement were also carried out. The studies revealed the presence of a major membrane protein (MMP) (shed via passive protein leakage) in the sample suspensions that was targeted by the monoclonal antibody. The implications of this finding (i.e., the ability to selectively capture and label shed membrane proteins) with respect to its potential to function as a facile, intrinsic amplification pathway for high-sensitivity assays for *M. avium* subsp. *paratuberculosis* and other cells and viruses are also briefly discussed.

MATERIALS AND METHODS

Bacterium preparation. *M. avium* subsp. *paratuberculosis* K-10 bacteria were cultured at the National Animal Disease Center (Ames, IA) in Middlebrook 7H9 medium (Becton Dickinson, Cockeysville, MD) that was supplemented with 2 mg/liter mycobactin J (Allied Monitor Inc., Fayette, MO), 10% oleic acid albumin–dextrose complex (Becton Dickinson), and 0.05% Tween 80 (Sigma-Aldrich, St. Louis, MO) (54). The bacilli were removed by centrifugation (10,000 × *g* for 20 min), washed with cold phosphate-buffered saline solution (PBS) (0.15 M, pH 7.2), and heat treated at 80°C for 30 min. To avoid clumping, the bacterial suspension was repeatedly (10 times) passed through a 16-gauge needle, placed into a 15-ml tube, and allowed to settle stagnantly for 10 min. The top half of this solution was then removed and heat killed with the resulting suspension used in all assays as well as in all determinations of bacterial concentrations. Heat-killed, whole-cell bacterial concentrations were determined by flow cytometry using a Live/Dead Bac*Light* bacterial viability and counting kit (Molecular Probes, Eugene, OR). These measurements yielded an average value of $1.3 \times 10^7 \pm 0.3 \times 10^7$ *M. avium* subsp. *paratuberculosis* cells/ml for dead bacilli with no live bacilli present. These values were further verified by stationary culturing of live *M. avium* subsp. *paratuberculosis* cells and serial dilution plating onto Herrold's egg yolk slants containing mycobactin J (2 mg/liter).

Spiked PBS and whole milk samples. Antigen solutions were prepared at room temperature by serial dilution of the *M. avium* subsp. *paratuberculosis* stock suspensions with either PBS (pH 7.4) (10 mM powder packs; Sigma-Aldrich) or pasteurized, whole milk (purchased from a local retailer but not tested for the presence of *M. avium* subsp. *paratuberculosis* prior to use). Between each dilution, cell suspensions were briefly vortexed to ensure homogeneity. Distilled water, subsequently deionized with an 18 MΩ Milli-Q system (Millipore, Billerica, MA), was used for the preparation of all aqueous reagents. For the milk matrix, the initial dilution added 10 μl of 10^7 *M. avium* subsp. *paratuberculosis* cells/ml in PBS to 90 μl of whole milk.

Antibodies. Monoclonal antibody (mAb) 13E1 targets the MMP MAP2121c (2). The MAP2121c protein was recombinantly produced in *Escherichia coli* cells and subsequently used to immunize mice for the production of mAbs (3). 13E1 was then purified from tissue culture supernatants at the Iowa State University

Hybridoma Facility using Melon gel (Pierce, Rockford, IL). The 13E1 concentration was determined by spectrophotometric measurements at 280 nm with an ε value of 13.7 liters g^{-1} cm^{-1} (ND-1000; NanoDrop, Wilmington, DE). All dilutions of 13E1 employed 50 mM borate buffer (pH 8.3 borate buffer packs; Pierce).

ERL preparation. Previous reports detailed the preparation of ERLs (15, 54). Briefly, 1.0 ml of 60-nm gold particles (<8% variation in diameter, 2.6×10^{10} particles/ml; Ted Pella, Redding, CA) was mixed with 40 μl of 50 mM borate buffer (pH 8.3). This step was followed by the addition of 10 μl of 1 mM 5,5′-dithiobis(succinimidyl-2-nitrobenzoate) (DSNB) in acetonitrile (high-performance liquid chromatography grade; Fisher, Pittsburgh, PA). DSNB coats the nanoparticles as an adlayer of a gold-bound thiolate and serves both as the Raman scatterer for readout and as the linker molecule for antibody attachment. After 7 h of incubation, 20 μg of 13E1 was added and reacted for ~12 h, a step which tethers the mAb to the DSNB-derived coating via an amide linkage (16, 25, 51). Finally, 100 μl of 10% bovine serum albumin (Sigma-Aldrich) in 2 mM borate buffer was pipetted into the suspension and reacted for 7 h to block unreacted succinimidyl esters.

For the removal of excess reagents, the colloidal suspension was centrifuged (MiniSpin; Eppendorf, Westbury, NY) at 2,000 × *g* for 10 min. The supernatant solution was then removed, and the loose ERL pellet was resuspended in 1,000 μl of 2 mM borate buffer containing 1% bovine serum albumin. This process was repeated twice to maximize the removal of unreacted materials, with a final resuspension volume of 500 μl. The next step added 50 μl of 10% (wt/vol) sodium chloride (Sigma-Aldrich) to the suspension to mimic biological conditions. Finally, to remove any large clusters of nanoparticles, the solution was passed through a 0.22-μm syringe filter (Costar, Fisher).

Capture surface formation. The capture substrates were constructed according to protocols described previously (15, 23, 35, 36, 54). Gold substrates were prepared by resistive evaporation of ~300 nm of 99.9% pure gold at 0.1 to 0.2 nm/s onto a 4-in. P-type test-grade silicon [111] wafer (University Wafer, South Boston, MA) using an Edwards 306A vacuum deposition system. Cleaned 1- by 1-cm glass chips were then gently affixed to the gold surface via two-part epoxy (Epo-tek 377) and cured at 150°C for 1.75 h. The separation of glass chips from the wafer exposed the underlying gold surface. The gold surfaces were modified by forming a hydrophobic barrier that surrounds the assay address. To this end, an octadecanethiol (Sigma-Aldrich)-coated, poly(dimethyl siloxane) (Dow Corning, Midland, MI) stamp, with a 3.2-mm-diameter centered hole, was used to ink the gold surface. The substrates were then exposed to a 0.1 mM ethanolic (Aaper, Shelbyville, KY) solution of dithiobis(succinimidyl propionate) (DSP) (Sigma-Aldrich) for 14 h. After rinsing the substrates with ethanol and drying under a stream of high-purity nitrogen, 20 μl of 13E1 (100 μg/ml) was pipetted onto the substrate and reacted for 7 h. This step linked the mAb to the substrate by the same mechanism as that used in the ERL preparation. The slides were then rinsed three times with 2 ml of 10 mM PBS buffer. Finally, unreacted succinimidyl end groups were capped with SuperBlock (20-μl drop; Pierce).

Immunoassay protocol. The capture substrates were exposed to various concentrations of heat-killed, whole-cell *M. avium* subsp. *paratuberculosis* (referred to hereafter simply as *M. avium* subsp. *paratuberculosis*) in 10 mM PBS buffer (pH 7.4) or pasteurized, whole milk. After incubation at room temperature in a humidity chamber for 7 h, the substrates were washed three times with 2 mM borate buffer (pH 8.3) with 150 mM NaCl. Next, the captured antigen was labeled with ERLs (20-μl drop) through a 14-h incubation step. Finally, the surfaces were rinsed with borate buffer and gently dried with nitrogen.

SERS measurements (i) NanoRaman I. SERS spectra for the immunoassay were collected using a NanoRaman I spectrometer (Concurrent Analytical, Waimanalo, HI) with a HeNe laser (632.8 nm, 30-mW output), a fiber optic-based probe head, an *f*/2.0 Czerny-Turner imaging spectrometer (6- to 8-cm^{-1} resolution), and a 0°C thermoelectrically cooled charge-coupled device (Kodak 0401E). Normal-incidence laser light was focused onto the substrate surface via a 0.68-numerical-aperture objective (25-μm-diameter spot, 2 to 3 mW at the surface), and exposure times of either 1 or 5 s were employed. The same objective and fiber optic probe collected the scattered radiation. All the data points in the resulting calibration curves are the averages of five measurements at different locations on each capture substrate.

(ii) Raman microscope. The samples were also examined by using an in-house Raman spectroscopy microscope. This system was composed of an optical microscope (Olympus BH-2) and a spectrograph (SpectraPro 300i; Acton Research, Acton, MA) that was connected to a thinned, back-illuminated, liquid nitrogen-cooled charge-coupled device (LN/CCD-1100PB; Princeton Instruments, Trenton, NJ). For spectral measurements, a 60-mW HeNe laser (632.8 nm) was attenuated through a variable, neutral-density filter (Thorlabs, Newton, NJ). The substrate was mounted onto the microscope sample stage, and laser light was focused through a 100× objective to form a ~1.5-μm-diameter spot size at an incident power of ~1 mW. The scattered light was collected through the same objective and directed to the spectrograph. All the microscopy-based spectra were collected with a 2-s integration time via WinSpec/32 (Princeton Instruments), and microscope images were obtained with ATI Multimedia video software (ATI Technologies, Markham, Ontario, Canada).

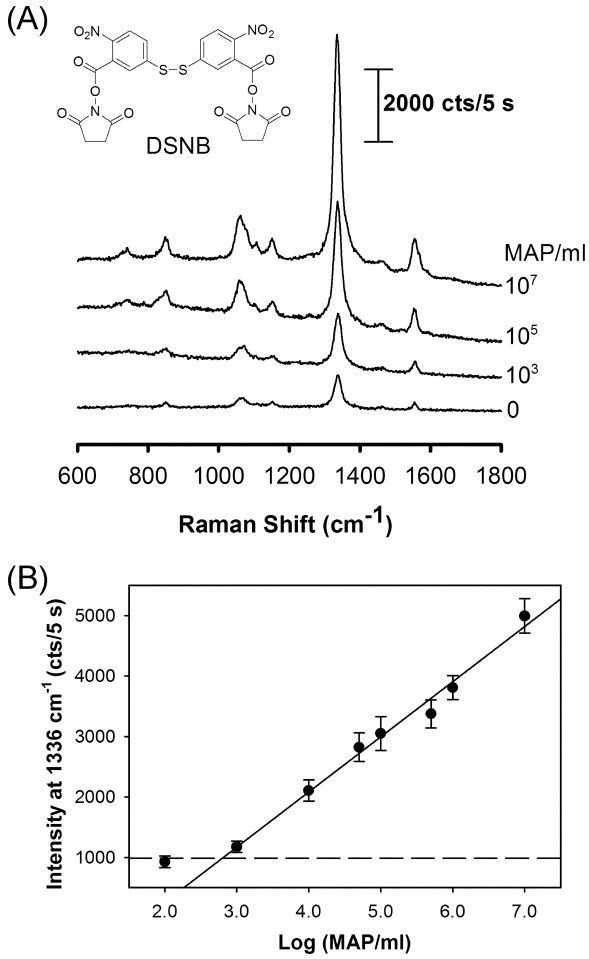

FIG. 2. SERS spectra and calibration curve for *M. avium* subsp. *paratuberculosis* (MAP)-spiked PBS samples. Spectra (vertically offset for clarity) with intensity in counts (cts) per 5 s (A) and corresponding calibration curve using $\nu_s(NO_2)$ intensity (B) are shown. The dashed line corresponds to the blank plus three times its standard deviation. The best-fit line is as follows: $y = 913x - 1{,}568$ ($R^2 = 0.98$).

SEM imaging. Scanning electron microscopy (SEM) images were obtained using a JEOL (Tokyo, Japan) 59101v instrument. Each sample was sputter coated with a thin layer of gold prior to loading into the SEM chamber. A working distance of 10 mm and an accelerating voltage of 15 kV were used. All the images herein are from secondary electrons.

RESULTS

Assay of *M. avium* subsp. *paratuberculosis* in PBS. As detailed in Materials and Methods, *M. avium* subsp. *paratuberculosis* dilutions in PBS were incubated with the capture substrate, exposed to the ERLs, and read out with an integration time of 5 s (Fig. 1B1 and C1). The overall process was completed in fewer than 24 h. The resulting SERS spectra and calibration curve are presented in Fig. 2. All the spectral features evident in Fig. 2A are consistent with vibrational modes

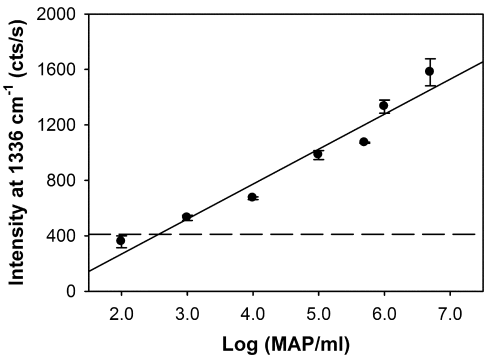

FIG. 3. SERS-based calibration curve for whole-cell *M. avium* subsp. *paratuberculosis* (MAP) in a milk matrix. The same trend was described in the legend of Fig. 2 (1-s integration; $y = 281x - 395$; $R^2 = 0.95$), with increasing SERS intensity with increasing *M. avium* subsp. *paratuberculosis* concentrations. The dashed line corresponds to the blank plus three times its standard deviation. cts/s, counts per second.

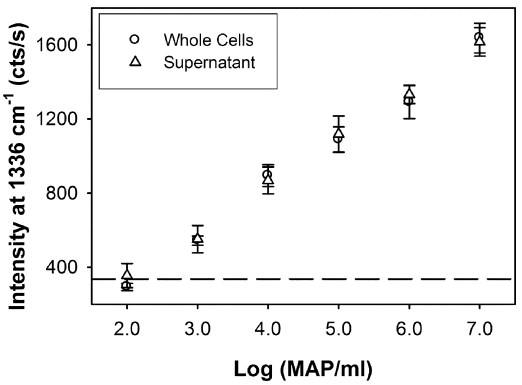

FIG. 4. SERS intensity of whole-cell *M. avium* subsp. *paratuberculosis* (MAP) suspensions compared to that of its extract (i.e., supernatant of these suspensions after bacteria have been pelleted out). The points from the two assays, whole-cell *M. avium* subsp. *paratuberculosis* and supernatant without *M. avium* subsp. *paratuberculosis*, strongly coincide. The dashed line corresponds to the blank plus three times its standard deviation. cts/s, counts per second.

for the DSNB-derived monolayer that coats the ERLs. The strongest band in the spectra is at 1,336 cm^{-1} and is attributed to a symmetric nitro stretch, $\nu_s(NO_2)$, whereas the weaker bands at 1,062 and 1,554 cm^{-1} are assigned to aromatic ring modes. In accordance with data shown in Fig. 1, the SERS intensities should track with the amount of bacteria in the antigen suspension, and this trend is observed in Fig. 2A.

To create the calibration curve shown in Fig. 2B, the SERS intensity in each spectrum was calculated by subtracting the background at 1,225 cm^{-1} from the signal maximum at 1,336 cm^{-1} and plotted as a function of the *M. avium* subsp. *paratuberculosis* concentration. The plot follows the above-mentioned trend in that the SERS intensity increases with *M. avium* subsp. *paratuberculosis* concentration. It also has a linear dynamic range, discussed in more detail below, that spans at least 4 orders of magnitude. The lowest detectable signal, defined as the blank (negative control) signal plus three times its standard deviation, is marked by the dashed line on the calibration plot. The intersection of this line with the linear best fit to the data defines the limit of detection (LOD), which is ~630 *M. avium* subsp. *paratuberculosis* cells/ml in this assay.

Assay of *M. avium* subsp. *paratuberculosis* in whole milk. To assess performance in more complex matrices, milk was spiked with *M. avium* subsp. *paratuberculosis* at concentrations ranging from 0 to 5.0×10^6 *M. avium* subsp. *paratuberculosis* cells/ml. These assays were done according to the procedure described above for PBS but employed a readout time of 1 s. The resulting calibration curve is shown in Fig. 3. Interestingly, the LOD in the whole milk matrix is ~740 *M. avium* subsp. *paratuberculosis* cells/ml, which is only slightly larger than that found when PBS was used. Moreover, the results for PBS (Fig. 2) and whole milk (Fig. 3), as judged by the best-fit lines, *y* intercept, and precision are strikingly similar after taking into account the difference in integration times (i.e., 5 s for spiked PBS and 1 s for spiked milk). This close correspondence argues that the complex whole milk matrix does not compromise the performance of the *M. avium* subsp. *paratuberculosis* assay.

Investigation of MMP shedding. While the performance of this novel assay platform is potentially applicable to many of the multifaceted needs for *M. avium* subsp. *paratuberculosis* detection, a more in-depth examination of the data (e.g., LOD) raises questions as to the origins of the results. As discussed in detail below, the theoretical LOD for the SERS-based assay is $\sim 8 \times 10^5$ cells/ml. However, the experimentally determined LOD is more than 3 orders of magnitude lower than this prediction. This discrepancy led to the following investigations for the basis of the apparent enhancement in performance and, specifically, the presence of MAP2121c as shed protein in the sample suspensions.

Two experiments were performed to determine if free MAP2121c was present in the bacterial suspension, which would potentially contribute to the response via the pathway depicted in Fig. 1B2 and C2. The first experiment was carried out using *M. avium* subsp. *paratuberculosis*-containing suspensions before and after the removal of *M. avium* subsp. *paratuberculosis* bacilli. The second study used capture substrates that had been exposed to suspensions containing bacteria and subsequently interrogated with a Raman microscope. This microscope has a focused laser spot that is comparable in size to that of an *M. avium* subsp. *paratuberculosis* bacillus and can therefore be used for the characterization of the SERS response in specific areas with and without bacteria present.

For both tests, one set of substrates was exposed to *M. avium* subsp. *paratuberculosis*-containing suspensions (20 μl). The remaining solutions were then centrifuged at 7,000 rpm (~3,300 × *g*) for 10 min to pellet out the bacteria. Next, 20 μl of the resulting supernatant (extracts) was pipetted onto a second set of capture substrates. After completing the incubations with the antigenic solutions and ERLs, the SERS responses and optical microscope images of each sample were obtained. The optical microscope images (data not shown) revealed that (i) bacteria were bound to the substrates that were exposed to the whole-cell *M. avium* subsp. *paratuberculosis* suspensions and (ii) no bacteria were detectably captured on the substrates that were treated with only the extracts. These results indicate that the centrifugation step effectively removes most of the *M. avium* subsp. *paratuberculosis* microorganism from extracts.

Figure 4 summarizes the data obtained from the two sets of assays as plots of the SERS intensities for $\nu_s(NO_2)$ versus the

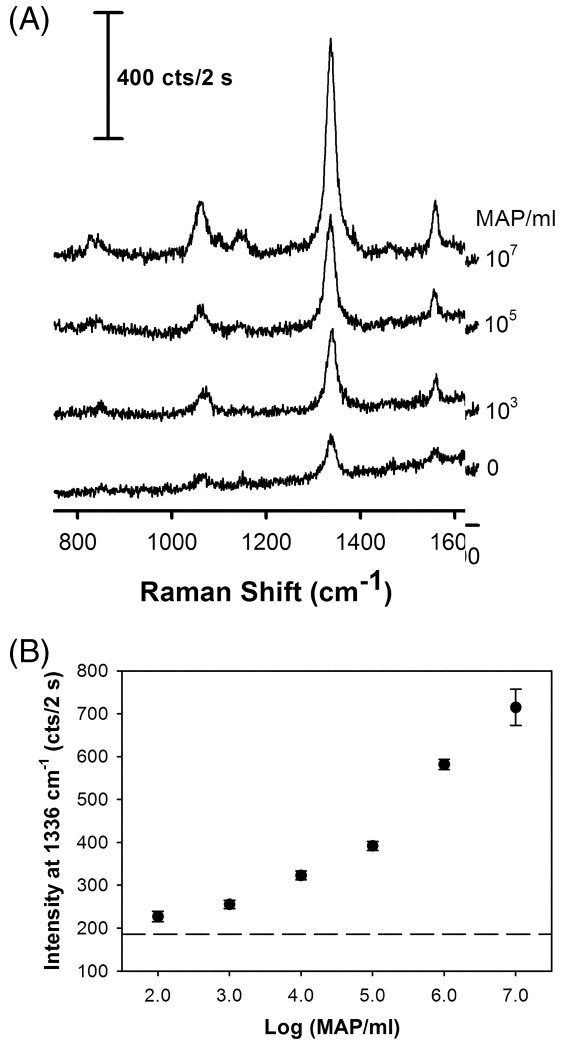

FIG. 5. (A) SERS spectra vertically offset for clarity. (B) Corresponding calibration curve from Raman microscope measurements of areas between bacteria on the assay substrate. Signals from areas devoid of bacteria increased with increased *M. avium* subsp. *paratuberculosis* (MAP) concentrations in the antigen suspensions, indicating that ERLs were specifically bound to the substrate surface. The dashed line corresponds to the blank plus three times its standard deviation. cts, counts.

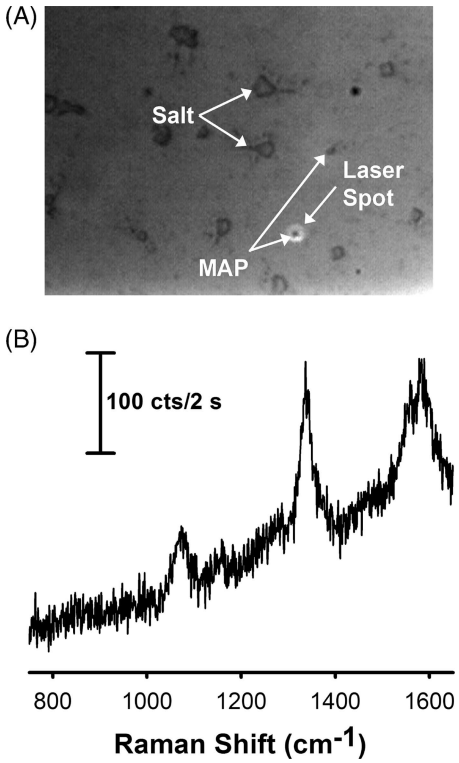

FIG. 6. (A) Laser spot from a 100× objective over a single bacterium. (B) SERS spectrum from the single bacterium with bound ERLs obtained with the Raman microscope. The bacterium had a SERS spectrum containing the distinct spectral features of the DSNB-derived Raman reporter, indicating that ERLs were also bound to the bacteria. MAP, *M. avium* subsp. *paratuberculosis*; cts, counts.

original *M. avium* subsp. *paratuberculosis* concentrations. The two plots, both of which exhibit an increase in signal with *M. avium* subsp. *paratuberculosis* concentration, are virtually indistinguishable. These findings agree with the protein shedding hypothesis. In other words, not only is the MMP MAP2121c present in the whole-cell suspensions, it can also be captured and labeled. Furthermore, the remarkably strong similarity of the two plots argues that shed protein is the overwhelming contributor to the observed responses for the whole-cell suspensions.

The second experiment tested the shedding hypothesis further by using an in-house-built Raman microscope and the capture substrates exposed to whole-cell *M. avium* subsp. *paratuberculosis*. With this instrument, the capture substrate can be positioned using the sample stage under the 1.5-μm laser focus, providing a means to evaluate either the signature of a captured bacterium or an area of the substrate devoid of bacilli. When the laser illuminated a location free of bacteria, the SERS spectra and calibration curve shown in Fig. 5 were obtained. The spectra in Fig. 5A not only have features characteristic of the DSNB-based label but also undergo intensity changes in line with the amount of bacteria in the antigen suspensions prior to centrifugation. This trend is also evident in the calibration curve shown in Fig. 5B, in which the data points are an average of three measurements at different locations on each of the individual capture substrates.

When the laser beam is focused on a single bacterium (Fig. 6A), a weak, but distinct, spectrum is obtained (Fig. 6B). While having a few bands indicative of the Raman reporter molecule, the spectrum also has a broad feature at 1,600 cm^{-1}, which we believe originates from the underlying microorganism (55). The response of individual bacilli from several substrates was then characterized. This study yielded an average intensity for the $\nu_s(NO_2)$ of only 170 ± 11 counts/2 s (n = 11 bacilli). There are two important conclusions that can be drawn from these results. First, captured bacteria generate a SERS response after ERL labeling. Second, the response is much smaller than that observed when interrogating locations devoid of bacilli. In fact, the signal strength from an intact bacterium is on par with that from the blank spectrum shown in Fig. 5. These observations are consistent with the overlay of the two plots in Fig. 4

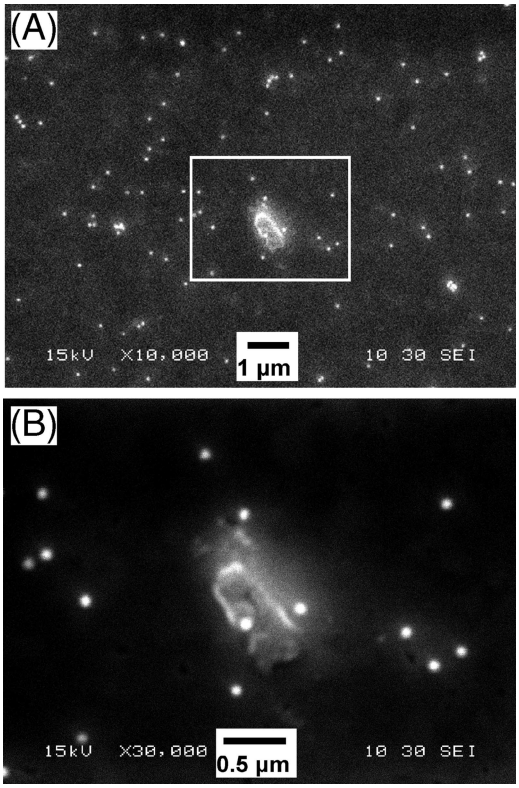

FIG. 7. SEM images of an assay platform exposed to 1.3×10^7 *M. avium* subsp. *paratuberculosis* cells/ml and 60-nm ERLs with bacterium in the center (A) and an expanded area from the box in A (B). Results visually confirm spectroscopy measurements in Fig. 5 and 6.

and are again an indication that any captured whole-cell *M. avium* subsp. *paratuberculosis* has, at best, a minor contribution to the SERS signal.

Lastly, these samples were imaged by SEM to cross-correlate the location of the ERLs and bacteria on the capture substrate. The samples were therefore briefly rinsed with deionized water to remove salt residue, dried, sputter coated with gold, and imaged. Shown in Fig. 7 are SEM images (~12 by 9 μm and ~4 by 3 μm) of a capture substrate that was exposed to 1.3×10^7 *M. avium* subsp. *paratuberculosis* cells/ml. A single bacterium, identified by its rod-like shape (~1 by 0.5 μm), is evident in the center of both images. There are also several smaller, circular objects that have a size consistent with the 60-nm gold core of the ERLs. There is, however, no apparent preference for ERLs to be in close proximity to the captured microorganism; that is, while there are a few ERLs close enough to the microorganism to be interrogated by the laser beam when it is focused on a single bacillus, most of the nanoparticles on the surface are clearly positioned outside the irradiated region. Moreover, there were no visible bacteria and very few nonspecifically bound ERLs (~15 in 100 μm^2) on blank samples in comparison to the slides containing *M. avium* subsp. *paratuberculosis* bacilli (10^7 *M. avium* subsp. *paratuberculosis* cells/ml substrate had ~125 ERLs in 100 μm^2). These findings further support the likelihood that shed protein is captured by the substrate and that the majority of the response for the whole-cell *M. avium* subsp. *paratuberculosis* assay arises from ERLs bound to shed protein and not captured bacteria.

In summary, these studies yield three important conclusions: (i) there is shed protein on the assay surface, (ii) the amount of protein increases as the original amount of bacteria in the suspension increases, and (iii) captured, shed protein can bind ERLs.

DISCUSSION

The work herein, which was designed to build on the assay for *M. avium* subsp. *paratuberculosis* sonicate described in the companion paper (54), has demonstrated the apparent ability to quantitate heat-killed, whole-cell *M. avium* subsp. *paratuberculosis* in fewer than 24 h and at LODs of ~630 *M. avium* subsp. *paratuberculosis* cells/ml in PBS and ~740 *M. avium* subsp. *paratuberculosis* cells/ml in whole milk. While we need to push performance to a higher sensitivity to address the need for subclinical levels of detection, this work is our first step toward the creation of a platform for the direct evaluation of bacterium levels in milk. This approach has LODs that are comparable to that recently obtained (~500 CFU/ml) by Stratmann and coworkers, who applied a new peptide-mediated capture PCR method to artificially contaminated milk (47), but the SERS readout immunoassay may potentially be in a more easy-to-use format.

We noted previously, however, that the LOD for this *M. avium* subsp. *paratuberculosis* assay is over 3 orders of magnitude lower than theoretical expectations. The theoretical detection limit for this assay can be approximated by assuming that the lowest level of detection corresponds to a single bacterium present in the laser spot. Since the surface area of the capture substrate is defined by its 3.2-mm diameter, and the laser spot has a diameter of 25 μm, one bacillus per laser spot corresponds to 1.6×10^4 cells per capture address. This number of bacteria, when placed into a 20-μl sample droplet, translates to a detection limit of 8.2×10^5 cells/ml. The projected theoretical LOD is therefore over 1,000 times greater than the experimentally determined LOD of ~700 *M. avium* subsp. *paratuberculosis* cells/ml. It is precisely this issue that triggered the investigations that confirmed the presence of the shed MMP (i.e., MAP2121c) targeted by the 13E1 mAb.

The next question rests with the mechanistic origin of shed MMP. Is the protein actively secreted by the bacillus, or is passive shedding induced by sample preparation? Other mycobacteria, specifically *Mycobacterium bovis* BCG, are known to release cell wall lipids (39). However, MAP2121c has no signal sequence to suggest secretion and has previously been shown to be associated with the cell membrane (2). It would nonetheless be invaluable to determine if live mycobacteria actively secrete protein, and experiments along this line will be carried out in the near future.

We believe that the observed shedding is caused by our sample preparation methods, with the surface protein being stripped from the bacteria during heat treatment and/or by the vortexing step used when mixing the spiked PBS and milk samples. In fact, a recent study has shown that surface proteins can be readily detached from *M. avium* subsp. *paratuberculosis* by brief sonication (43). It is possible that the vortexing step used in our sample preparation does exactly that. Nonetheless,

shedding leads to an effective approach to signal amplification from individual cells and is central to the ~1,000-fold improvement in the observed detection limits with respect to the theoretical prediction.

These results point to an intriguing new strategy to increase the sensitivity and specificity of various diagnostic tests by harnessing protein shedding. Since other *M. avium* subsp. *paratuberculosis* proteins may also be shed, either actively or passively, an approach to enhance the specificity and sensitivity of a test for *M. avium* subsp. *paratuberculosis* could potentially be devised by the concurrent detection of several different surface proteins. To this end, work to further evaluate the shedding process and extend the concept of multiple-protein detection is currently under way. In addition, efforts to investigate the applicability of the concept to other bacteria as a general mechanism for signal amplification are planned.

Another intriguing aspect of this *M. avium* subsp. *paratuberculosis* assay is its large linear dynamic range, which is at least 5 orders of magnitude on the log scale. Simple equilibrium models of two-site immunoassays predict a linearity of only 3 orders of magnitude in antigen concentration (13). As discussed previously by Plowman et al. (38), larger dynamic ranges can arise by the existence of two different ligand-receptor interactions, for example, in the capture step. Thus, the breadth of the dynamic range would be larger than that typically predicted because the stronger interaction would dominate binding at the lower concentrations, followed by capture at sites with the lower binding strength. Although we are as yet uncertain as to how two distinct binding constants would arise in this case, steric effects from two mAbs binding to the same epitope could possibly allow for the different values. Indeed, preliminary results from calculations based on the Plowman model for the MMP-13E1 interaction (i.e., one strong and one weak binding constant) show that the linear dynamic range of the assay can be extended by another 2 to 3 orders of magnitude. Work to fully model these findings is ongoing and will be reported elsewhere.

In conclusion, the performance of the heat-killed, whole-cell *M. avium* subsp. *paratuberculosis* assay is dominated by the presence of shed surface protein. Due in part to this amplification, this assay allows for a rapid, selective, and sensitive test that can translate to complex sample matrices and thus possibly improve upon current diagnostic tests for Johne's disease. In addition, the quantitative nature of this assay may enable further refinement in definitions of disease stages and progression. Further studies aimed at translating the method to a test kit for use in diagnostic laboratories are under way. Finally, research to detect *M. avium* subsp. *paratuberculosis* in fecal samples as well as monitoring *M. avium* subsp. *paratuberculosis* levels in controlled Johne's disease herds are in progress.

ACKNOWLEDGMENTS

We acknowledge Rachel Millen for expert assistance in obtaining the SEM images, Jeremy Driskell for valuable discussions, and the insightful input of one of the reviewers.

This work was supported by the Institute for Combinatorial Discovery of Iowa State University and by a grant from CEROS/DARPA. The Ames Laboratory is operated for the U.S. Department of Energy by Iowa State University under contract no. DE-AC02-07CH11358. We also acknowledge support from the USDA-NRI-CAP JDIP program to J.P.B. as well as support from the USDA's Agricultural Research Service.

REFERENCES

1. **Ansari, D. O., D. A. Stuart, and S. Nie.** 2005. Surface-enhanced Raman spectroscopic detection of cancer biomarkers in intact cellular specimens. Proc. SPIE **5699:**82–90.
2. **Bannantine, J. P., J. F. Huntley, E. Miltner, J. R. Stabel, and L. E. Bermudez.** 2003. The Mycobacterium avium subsp. paratuberculosis 35 kDa protein plays a role in invasion of bovine epithelial cells. Microbiology **149:**2061–2069.
3. **Bannantine, J. P., T. J. Radosevich, J. R. Stabel, S. Berger, J. F. Griffin, and M. L. Paustian.** 2007. Production and characterization of monoclonal antibodies against a major membrane protein of *Mycobacterium avium* subsp. *paratuberculosis*. Clin. Vaccine Immunol. **14:**312–317.
4. **Beard, P. M., M. J. Daniels, D. Henderson, A. Pirie, K. Rudge, D. Buxton, S. Rhind, A. Greig, M. R. Hutchings, I. McKendrick, K. Stevenson, and J. M. Sharp.** 2001. Paratuberculosis infection of nonruminant wildlife in Scotland. J. Clin. Microbiol. **39:**1517–1521.
5. **Beard, P. M., S. M. Rhind, D. Buxton, M. J. Daniels, D. Henderson, A. Pirie, K. Rudge, A. Greig, M. R. Hutchings, K. Stevenson, and J. M. Sharp.** 2001. Natural paratuberculosis infection in rabbits in Scotland. J. Comp. Pathol. **124:**290–299.
6. **Burton, M. S., J. H. Olsen, R. L. Ball, and G. A. Dumonceaux.** 2001. Mycobacterium avium subsp. paratuberculosis infection in an addax (Addax nasomaculatus). J. Zoo Wildl. Med. **32:**242–244.
7. **Cao, Y. C., R. Jin, and C. A. Mirkin.** 2002. Nanoparticles with Raman spectroscopic fingerprints for DNA and RNA detection. Science **297:**1536–1540.
8. **Clarke, C. J., I. A. Patterson, K. E. Armstrong, and J. C. Low.** 1996. Comparison of the absorbed ELISA and agar gel immunodiffusion test with clinicopathological findings in ovine clinical paratuberculosis. Vet. Rec. **139:**618–621.
9. **Colgrove, G. S., C. O. Thoen, B. O. Blackburn, and C. D. Murphy.** 1989. Paratuberculosis in cattle: a comparison of three serologic tests with results of fecal culture. Vet. Microbiol. **19:**183–187.
10. **Collins, M. T., S. J. Wells, K. R. Petrini, J. E. Collins, R. D. Schultz, and R. H. Whitlock.** 2005. Evaluation of five antibody detection tests for diagnosis of bovine paratuberculosis. Clin. Diagn. Lab. Immunol. **12:**685–692.
11. **Cousins, D. V., R. Whittington, I. Marsh, A. Masters, R. J. Evans, and P. Kluver.** 1999. Mycobacteria distinct from Mycobacterium avium subsp. paratuberculosis isolated from the feces of ruminants possess IS900-like sequences detectable by IS900 polymerase chain reaction: implications for diagnosis. Mol. Cell. Probes **14:**431–442.
12. **Dargatz, D. A., B. A. Byrum, L. K. Barber, R. W. Sweeney, R. H. Whitlock, W. P. Shulaw, R. H. Jacobson, and J. R. Stabel.** 2001. Evaluation of a commercial ELISA for diagnosis of paratuberculosis in cattle. J. Am. Vet. Med. Assoc. **218:**1163–1166.
13. **Diamandis, E. P., and T. K. Christopoulos (ed.).** 1996. Immunoassay. Academic Press, San Diego, CA.
14. **Dou, X., T. Takama, Y. Yamaguchi, and H. Yamamoto.** 1997. Enzyme immunoassay utilizing surface-enhanced Raman scattering of the enzyme reaction product. Anal. Chem. **69:**1492–1495.
15. **Driskell, J. D., K. M. Kwarta, R. J. Lipert, M. D. Porter, J. D. Neill, and J. F. Ridpath.** 2005. Low-level detection of viral pathogens by a surface-enhanced Raman scattering based immunoassay. Anal. Chem. **77:**6147–6154.
16. **Duhachek, S. D., J. R. Kenseth, G. P. Casale, G. J. Small, M. D. Porter, and R. Jankowiak.** 2000. Monoclonal antibody-gold biosensor chips for detection of depurinating carcinogen-DNA adducts by fluorescence line-narrowing spectroscopy. Anal. Chem. **72:**3709–3716.
17. **Dukes, T. W., G. J. Glover, B. W. Brooks, J. R. Duncan, and M. Swendrowski.** 1992. Paratuberculosis in saiga antelope (Saiga tatarica) and experimental transmission to domestic sheep. J. Wildl. Dis. **28:**161–170.
18. **Ellingson, J. L. E., J. R. Stabel, W. R. Bishai, R. Frothingham, and J. M. Miller.** 2000. Evaluation of the accuracy and reproducibility of a practical PCR panel assay for rapid detection and differentiation of Mycobacterium avium subspecies. Mol. Cell. Probes **14:**153–161.
19. **Faulds, K., W. E. Smith, and D. Graham.** 2005. DNA detection by surface enhanced resonance Raman scattering (SERRS). Analyst **130:**1125–1131.
20. **Garrell, R. L.** 1989. Surface-enhanced Raman spectroscopy. Anal. Chem. **61:**401A–402A, 404A, 406A–408A, 410A–411A.
21. **Godfroid, J., C. Delcorps, L. M. Irenge, K. Walravens, S. Marche, and J. L. Gala.** 2005. Definitive differentiation between single and mixed mycobacterial infections in red deer (*Cervus elaphus*) by a combination of duplex amplification of p34 and f57 sequences and Hpy188I enzymatic restriction of duplex amplicons. J. Clin. Microbiol. **43:**4640–4648.
22. **Graham, D., B. J. Mallinder, D. Whitcombe, N. D. Watson, and W. E. Smith.** 2002. Simple multiplex genotyping by surface-enhanced resonance Raman scattering. Anal. Chem. **74:**1069–1074.
23. **Grubisha, D. S., R. J. Lipert, H. Y. Park, J. Driskell, and M. D. Porter.** 2003. Femtomolar detection of prostate-specific antigen: an immunoassay based

on surface-enhanced Raman scattering and immunogold labels. Anal. Chem. **75:**5936–5943.
24. **Harris, N. B., and R. G. Barletta.** 2001. *Mycobacterium avium* subsp. *paratuberculosis* in veterinary medicine. Clin. Microbiol. Rev. **14:**489–512.
25. **Jones, V. W., J. R. Kenseth, M. D. Porter, C. L. Mosher, and E. Henderson.** 1998. Microminiaturized immunoassays using atomic force microscopy and compositionally patterned antigen arrays. Anal. Chem. **70:**1233–1241.
26. **Judge, J., I. Kyriazakis, A. Greig, D. J. Allcroft, and M. R. Hutchings.** 2005. Clustering of *Mycobacterium avium* subsp. *paratuberculosis* in rabbits and the environment: how hot is a hot spot? Appl. Environ. Microbiol. **71:**6033–6038.
27. **Kelly, K. L., E. Coronado, L. L. Zhao, and G. C. Schatz.** 2003. The optical properties of metal nanoparticles: the influence of size, shape, and dielectric environment. J. Phys. Chem. B **107:**668–677.
28. **Kneipp, K., H. Kneipp, I. Itzkan, R. R. Dasari, and M. S. Feld.** 2002. Surface-enhanced Raman scattering and biophysics. J. Phys. Condens. Matter **14:**R597–R624.
29. **Kneipp, K., H. Kneipp, I. Itzkan, R. R. Dasari, and M. S. Feld.** 1999. Ultrasensitive chemical analysis by Raman spectroscopy. Chem. Rev. **99:** 2957–2975.
30. **Lambeth, C., L. A. Reddacliff, P. Windsor, K. A. Abbott, H. McGregor, and R. J. Whittington.** 2004. Intrauterine and transmammary transmission of Mycobacterium avium subsp. paratuberculosis in sheep. Aust. Vet. J. **82:** 504–508.
31. **Machackova-Kopecna, M., M. Bartos, M. Straka, V. Ludvik, P. Svastova, J. Alvarez, J. Lamka, I. Trcka, F. Treml, I. Parmova, and I. Pavlik.** 2005. Paratuberculosis and avian tuberculosis infections in one red deer farm studied by IS900 and IS901 RFLP analysis. Vet. Microbiol. **105:**261–268.
32. **Mackintosh, C. G., G. W. de Lisle, D. M. Collins, and J. F. Griffin.** 2004. Mycobacterial diseases of deer. N. Z. Vet. J. **52:**163–174.
33. **Mulvaney, S. P., M. D. Musick, C. D. Keating, and M. J. Natan.** 2003. Glass-coated, analyte-tagged nanoparticles: a new tagging system based on detection with surface-enhanced Raman scattering. Langmuir **19:**4784–4790.
34. **Muskens, J., D. Bakker, J. de Boer, and L. van Keulen.** 2001. Paratuberculosis in sheep: its possible role in the epidemiology of paratuberculosis in cattle. Vet. Microbiol. **78:**101–109.
35. **Ni, J., R. J. Lipert, G. B. Dawson, and M. D. Porter.** 1999. Immunoassay readout method using extrinsic Raman labels adsorbed on immunogold colloids. Anal. Chem. **71:**4903–4908.
36. **Park, H.-Y.** 2005. Chip-scale bioassays based on surface-enhanced Raman scattering: fundamentals and applications. Ph.D. thesis. Iowa State University, Ames.
37. **Park, H.-Y., R. J. Lipert, and M. D. Porter.** 2004. Single particle Raman measurements of gold nanoparticles used in surface-enhanced Raman scattering (SERS)-based sandwich immunoassays. Proc. SPIE **5593:**464.
38. **Plowman, T. E., W. M. Reichert, C. R. Peters, H. K. Wang, D. A. Christensen, and J. N. Herron.** 1996. Femtomolar sensitivity using a channel-etched thin film waveguide fluoroimmunosensor. Biosens. Bioelectron. **11:** 149–160.
39. **Rhoades, E., F.-F. Hsu, J. B. Torrelles, J. Turk, D. Chatterjee, and D. G. Russell.** 2003. Identification and macrophage-activating activity of glycolipids released from intracellular *Mycobacterium bovis* BCG. Mol. Microbiol. **48:**875–888.
40. **Rohr, T. E., T. Cotton, N. Fan, and P. J. Tarcha.** 1989. Immunoassay employing surface-enhanced Raman spectroscopy. Anal. Biochem. **182:**388–398.
41. **Schatz, G. C., and R. P. Van Duyne.** 1980. Image field theory of enhanced Raman scattering by molecules adsorbed on metal surfaces: detailed comparison with experimental results. Surf. Sci. **101:**425–438.
42. **Sergeant, E. S., R. J. Whittington, and S. J. More.** 2002. Sensitivity and specificity of pooled fecal culture and serology as flock-screening tests for detection of ovine paratuberculosis in Australia. Prev. Vet. Med. **52:**199–211.
43. **Speer, C. A., M. C. Scott, J. P. Bannantine, W. R. Waters, Y. Mori, R. H. Whitlock, and S. Eda.** 2006. A novel enzyme-linked immunosorbent assay for diagnosis of *Mycobacterium avium* subsp. *paratuberculosis* infections (Johne's disease) in cattle. Clin. Vaccine Immunol. **13:**535–540.
44. **Stabel, J. R.** 1998. Johne's disease: a hidden threat. J. Dairy Sci. **81:**283–288.
45. **Storset, A. K., I. Berg, and B. Djonne.** 2005. Evaluation of the gamma interferon test for diagnosis of paratuberculosis in goats. Vet. Immunol. Immunopathol. **107:**87–94.
46. **Storset, A. K., H. J. Hasvold, M. Valheim, H. Brun-Hansen, G. Berntsen, S. K. Whist, B. Djonne, C. M. Press, G. Holstad, and H. J. Larsen.** 2001. Subclinical paratuberculosis in goats following experimental infection. An immunological and microbiological study. Vet. Immunol. Immunopathol. **80:**271–287.
47. **Stratmann, J., K. Dohmann, J. Heinzmann, and G.-F. Gerlach.** 2006. Peptide aMptD-mediated capture PCR for detection of *Mycobacterium avium* subsp. *paratuberculosis* in bulk milk samples. Appl. Environ. Microbiol. **72:** 5150–5158.
48. **Stratmann, J., B. Strommenger, K. Stevenson, and G.-F. Gerlach.** 2002. Development of a peptide-mediated capture PCR for detection of *Mycobacterium avium* subsp. *paratuberculosis* in milk. J. Clin. Microbiol. **40:**4244–4250.
49. **Sweeney, R. W., R. H. Whitlock, S. McAdams, and T. Fyock.** 2006. Longitudinal study of ELISA seroreactivity to Mycobacterium avium subsp. paratuberculosis in infected cattle and culture-negative herd mates. J. Vet. Diagn. Investig. **18:**2–6.
50. **Vo-Dinh, T.** 1998. Surface-enhanced Raman spectroscopy using metallic nanostructures. Trends Anal. Chem. **17:**557–582.
51. **Wagner, P., M. Hegner, P. Kernen, F. Zaugg, and G. Semenza.** 1996. Covalent immobilization of native biomolecules onto Au(111) via N-hydroxysuccinimide ester functionalized self-assembled monolayers for scanning probe microscopy. Biophys. J. **70:**2052–2066.
52. **Whittington, R. J., I. B. Marsh, and R. H. Whitlock.** 2001. Typing of IS 1311 polymorphisms confirms that bison (Bison bison) with paratuberculosis in Montana are infected with a strain of Mycobacterium avium subsp. paratuberculosis distinct from that occurring in cattle and other domesticated livestock. Mol. Cell. Probes **15:**139–145.
53. **Xu, S., X. Ji, W. Xu, X. Li, L. Wang, Y. Bai, B. Zhao, and Y. Ozaki.** 2004. Immunoassay using probe-labelling immunogold nanoparticles with silver staining enhancement via surface-enhanced Raman scattering. Analyst **129:** 63–68.
54. **Yakes, B. J., R. J. Lipert, J. P. Bannantine, and M. D. Porter.** 2008. Detection of *Mycobacterium avium* subsp. *paratuberculosis* by a sonicate immunoassay based on surface-enhanced Raman scattering. Clin. Vaccine Immunol. **15:**227–234.
55. **Zeiri, L., and S. Efrima.** 2005. Surface-enhanced Raman spectroscopy of bacteria: the effect of excitation wavelength and chemical modification of the colloidal milieu. J. Raman Spectrosc. **36:**667–675.
56. **Zeman, E. J., and G. C. Schatz.** 1987. An accurate electromagnetic theory study of surface enhancement factors for silver, gold, copper, lithium, sodium, aluminum, gallium, indium, zinc, and cadmium. J. Phys. Chem. **91:** 634–643.
57. **Zhang, X., M. A. Young, O. Lyandres, and R. P. Van Duyne.** 2005. Rapid detection of an anthrax biomarker by surface-enhanced Raman spectroscopy. J. Am. Chem. Soc. **127:**4484–4489.